Mock TAC

Radio plasma bubbles in Abell 2052 and the Perseus cluster

Taylor Dibblee-Barkman

Abstract

AGN feedback is thought to be the primary cause of slowed cooling rates and star formation in galaxy cluster cores. This is evidenced by cavities in X-ray observations of a number of clusters, including Abell 2052 and the Perseus cluster. The detailed composition of radio plasma bubbles formed by AGN jets is still unknown. We propose using MUSTANG-2 on the Green Bank Telescope to measure the thermal Sunyaez Zel'dovich (tSZ) effect to determine whether the southern radio bubbles in Abell 2052 and Perseus are pressure-supported by hot thermal gas.

1 Science justification

1.1 X-ray cavities and radio plasma bubbles

Large cavities in the intracluster medium (ICM) have been observed for a number of clusters, including Perseus (Abell 426), Abell 2052, Abell 4059, Hydra-A cluster, etc. These cavities appear as deficits in X-ray emission maps (Blanton et al. (2011); Fabian et al. (2000)) which coincide with radio-bright bubbles that are inflated by jets of radio plasma from a cool core cluster's central active galactic nucleus (AGN). The cavities may also be due to "ghost bubbles", which are dim in radio signals because of the effect of relativistic electrons in the ICM (Hlavacek-Larrondo, Li, and Churazov (2022); Pfrommer, Ensslin, and Sarazin (2005)). Numerous high precision images of individual elliptical galaxies and galaxy clusters from the Chandra X-ray Observatory have revealed details in the ICM. These indicate that AGN feedback is the main driver of heating intracluster gas, which provides evidence to solve the "cooling flow problem": observations of the cooling rate of hot gas within a cluster's center are significantly lower than those given by predictions for the temperature and density of the ICM (Hlavacek-Larrondo et al. (2022); McDonald, Gaspari, McNamara, and Tremblay (2018)).

The detailed composition of radio bubbles is not known, but because the total pressure of observed bubbles is higher than the pressure due solely to cosmic ray electrons (CRes), the pressure support must be dominated by a combination of magnetic pressure, very hot thermal gas, hot thermal gas, cosmic ray protons (CRps), and relativistic CRes (Pfrommer et al. (2005); Yang, Gaspari, and Marlow (2019)). This can be described by two scenarios: one where the pressure is due to thermal effects, meaning the bubbles are supported by pressure from very hot thermal gas, and one where the pressure is due to non-thermal effects from the combination of relativistic CRes, CRps, and magnetic fields (Orlowski-Scherer et al. (2022)). Determining whether the radio bubbles contain very hot thermal gas may require more than X-ray observations alone because there may be low X-ray emissions depending on the bubbles' composition. High resolution SZ radio observations can complement X-ray observations. In particular, a detection or non-detection of tSZ signals can distinguish between the thermal and non-thermal scenarios (Pfrommer et al. (2005); Yang et al. (2019)).

1.2 The Sunyaev-Zel'dovich effect

The Sunyaev-Zel'dovich (SZ) effect arises from the inverse Compton scattering of CMB photons by electrons in the intracluster medium (ICM). This causes a shift in the blackbody spectrum to higher energies and frequencies. This is a scattering effect, meaning SZ is independent of redshift which makes it an ideal complement to X-ray and optical observations, which require longer exposure times at higher redshifts (Dicker et al. (2021); Mroczkowski et al. (2019)). The SZ effect can be broken down into different signals with different spectral and spatial dependencies in the cluster. The thermal SZ (tSZ) effect is due to scattering by electrons in regions of hot thermal gas and the kinematic SZ (kSZ) effect is due to the cluster's bulk motion relative to the CMB rest frame. tSZ and kSZ signals may need relativistic corrections, which are described by the relativistic SZ (rSZ) effect. The non-thermal SZ (ntSZ) effect is

due to non-thermal velocity distributions of electrons which can occur due to magnetic fields or turbulence, for example (Mroczkowski et al. (2019)).

The magnitude of the tSZ effect is proportional to electron pressure integrated along the line of sight. tSZ signals therefore reveal the dynamics of a cluster, relating the temperature/pressure/mass to structures such as shocks and bubbles. tSZ directly measures the thermal electron pressure in the ICM, so a sensitive measurement of tSZ can tell us whether or not the bubbles are supported by pressure from hot thermal gas (Dicker et al. (2021); Pfrommer et al. (2005)).

1.3 Abell 2052 and the Perseus cluster

Abell 2052 is a galaxy cluster at redshift $z = 0.0353$ with central coordinates *R.A.* (hr:min:sec) = 15:16:44.514, *Decl.* (deg:min:sec) = +07:01:17.02, and bolometric luminosity $L_{bol} = 10^{44}$ ergs/s (Cavagnolo (2009)). X-ray observations from Chandra show two distinct bubbles surrounded by bright X-ray rims, providing evidence that the cooling rate of gas is slower at the cluster's core (Blanton et al. (2011)). LOFAR observations of Abell 2052 found central radio sources in the X-ray cavities with lobes that do not extend far past the cavities (Bîrzan et al. (2020)).

The Persues cluster (Abell 426) is the brightest X-ray cluster with redshift $z = 0.0179$ with central coordinates *R.A.* (hr:min:sec) = 03:19:47.2 and *Decl.* (deg:min:sec) = +41:30:47 (Ebeling, Mullis, and Tully (2002)). It contains the radio source 3C 84 which blows bubbles of relativistic plasma into the cluster's core, shown by two cavities in X-ray images from Chandra (Fabian et al. (2000)). The combination of Chandra X-ray data and VLA data at 1.4 GHz suggest that the northern and southern X-ray cavities are supported by hot thermal gas. The northwest bubble in Perseus is a ghost bubble that has little high-frequency radio emissions (Seward and Charles (2010)). Perseus has a lower redshift and higher central temperature than Abell 2052, and therefore requires less integration time to detect the presence of a plasma bubble (Pfrommer et al. (2005)).

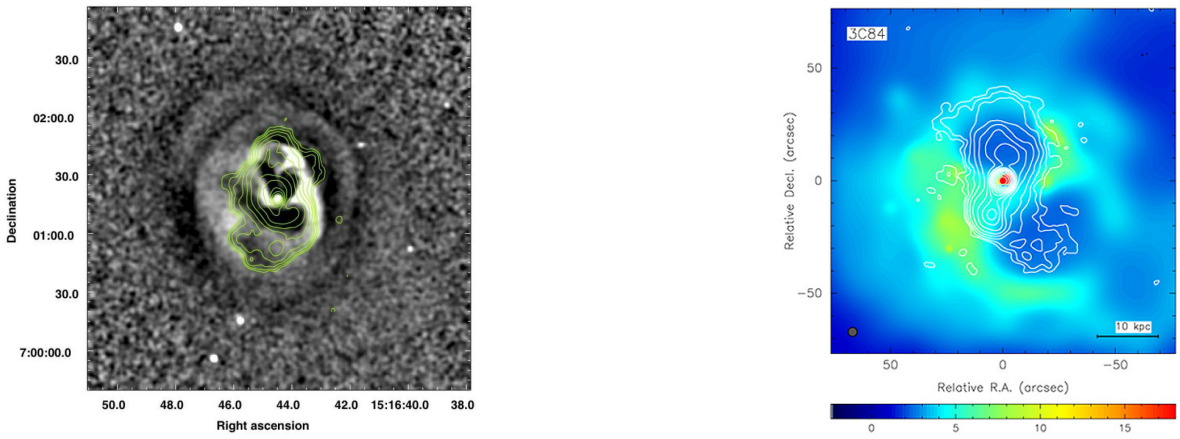

Figure 1: *(left)* Chandra X-ray image of Abell 2052 with 4.8 GHz contours overlaid (Blanton et al. (2011)). *(right)* Chandra X-ray image of the Perseus cluster with VLA radio contours overlaid (Fabian et al. (2000)).

These two low-redshift clusters (Fig. 1) with clearly defined X-ray cavities are ideal candidates for tSZ observations of radio plasma bubbles using MUSTANG-2. Pfrommer et al. (2005) performed synthetic observations of these clusters under different scenarios with the Green Bank Telescope (GBT) Penn Array Receiver, observing at 86-94 GHz. They investigated five different scenarios where the internal pressure of the cavities is dominated by different combinations of CRps, magnetic fields, ultra-relativistic CRes, trans-relativistic thermal proton and electron distributions, and dynamically dominant hot thermal gas (Pfrommer et al. (2005)).

2 Technical justification

2.1 MUSTANG-2 mapping speeds

The Multiplexed Squid TES Array at Ninety Gigahertz (MUSTANG-2 or M2) is a 223-feedhorn bolometer camera built for the Green Bank Telescope (GBT): a 100 m diameter radio telescope. M2 observes at 75-105 GHz and has an instantaneous field of view of 4 arcminutes and angular resolution of 9 arcseconds (FWHM) (Mason (2021); Romero (2021b); The Green Bank Observatory (2021)). M2's science goals include searching for substructures (bubbles, shocks) within galaxy clusters, measuring ICM profiles, searching for intercluster filaments, and follow-ups of previous cluster surveys (Dicker et al. (2021)). M2 uses a Lissajous daisy (LJD) scan method with varying radii. Mapping speed profiles are calculated based on 3000 LJD scans of different radii and assume a 45 degree observing elevation. The mapping speeds are based on the RMS within M2's central 2 arcminute radius circle. Regions with scan radii less than approximately 3 arcminutes have roughly uniform noise. Table 1 summarizes the M2 mapping speeds memo from Romero (2021a).

Table 1: M2 mapping speeds based on the RMS in central 2 arcminutes. Over small scan regions the noise is roughly uniform (Romero (2021a)).

Scan radius (arcminutes)	Mapping speed (μK$\sqrt{\text{hr}}$	Sensitivity (μJy/beam)
2.5	73	56.2
3.0	74	57
3.5	77	59.3
4.0	85	65.5
4.5	98	75.5
5.0	117	90.1

2.2 Observing times

Measurement requirements are based on synthetic GBT observations of Abell 2052 and the Perseus cluster from Pfrommer et al. (2005). These give simulated SZ flux decrements for both clusters, assuming the plasma bubbles contain ultra-relativistic electrons. Fig. 2 gives the desired sensitivity from the spacing of the radio contours, as well as estimates of the bubble diameters. Constraining the search to the clusters' southern cavities means less integration time in order to confirm whether tSZ signals are detectable from the plasma bubbles.

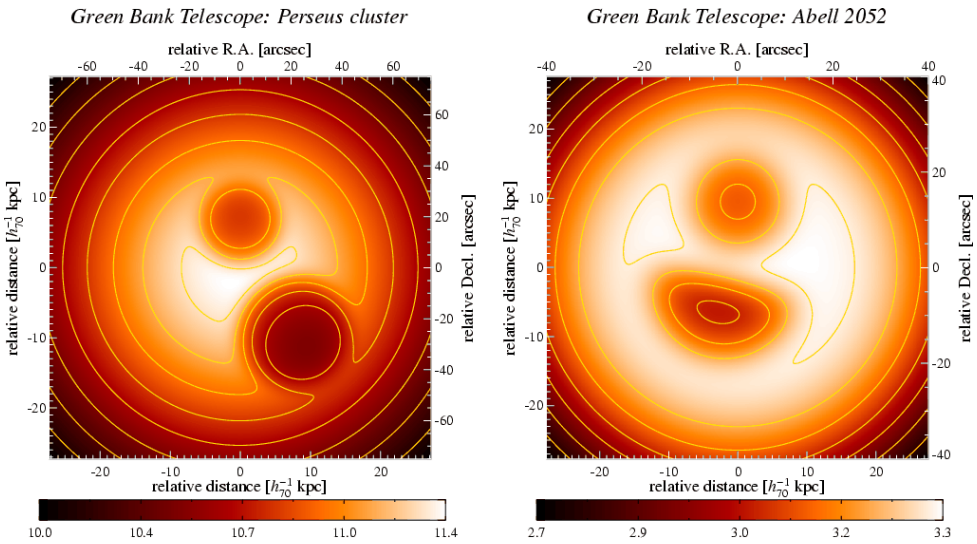

Figure 2: Synthetic GBT observations of Perseus *(left)* and Abell 2052 *(right)* at a 86-94 GHz frequency band. Simulated SZ flux decrement is in units of mJy/arcmin^2. The images are smoothed to the GBT 3 mm receiver's resolution of 8.0 arcsec (FWHM). The contour lines have a linear spacing of 0.16 mJy/arcmin^2 (Perseus) and 0.08 mJy/arcmin^2 (Abell 2052) (Pfrommer et al. (2005)).

The following describes the total integration time required for a 5σ detection of the southern bubble of Abell 2052. A LJD scan size of radius 2.5 arcmin, which has a corresponding mapping speed of 73 μK$\sqrt{\text{hr}}$ (Table 1), has a map area of 19.6 arcmin^2. For 18 hours of integration time, the integration time per square arcminute is 18 hr/19.6 arcmin^2 = 0.92 hr/arcmin^2. The expected map noise is therefore 73 μK$\sqrt{hr}/\sqrt{0.92 \text{ hr/arcmin}^2}$ = 76 μK-arcmin. The southern bubble of Abell 2052 is contained within a diameter of 20 arcsec, which gives an area of 0.09 arcmin^2. The measurement error on the amplitude of the bubble is therefore 76 μK-arcmin/$\sqrt{0.09 \text{ arcmin}^2}$ = 258 μK. We want to measure a flux decrement to within 80 μJy/arcmin^2.[1] Taking the M2 mapping speeds based on the RMS in the central 2 arcminutes, which convert from μK to μJy/beam by multiplying the μK noise by 0.77, this gives a desired sensitivity of 1005 μJy/beam = 1306 μK. For an integration time of 18 hr, the SNR is therefore 1306 μK/258 μK $\approx$ 5, meaning this should result in a 5σ detection. Note that M2 requires a 100% overhead relative to observing time (assume equal integration time and time to calibrate and general overheads), so we request a total observing time of 2×18 hr = 36 hr.

The calculation for a 5σ detection of the southern bubble of Perseus is nearly identical. The map area is once again 19.6 arcmin^2, which combined with an integration time of 4.5 hours gives an integration time per square arcminute of 4.5 hr/19.6 arcmin^2 = 0.23 hr/arcmin^2. The expected map noise is 73 μK$\sqrt{hr}/\sqrt{0.23 \text{ hr/arcmin}^2}$ = 152 μK-arcmin. The southern bubble of Perseus is contained within a diameter of approximately 20 arcseconds, once again giving an area of 0.09 arcmin^2. The measurement error is 152 μK-arcmin/$\sqrt{0.09 \text{ arcmin}^2}$ = 516 μK. To measure a flux decrement to within 160 μJy/arcmin^2, we require a M2 sensitivity of 2011 μJy/beam = 2611 μK. For a 5σ detection we have a SNR of 2611 μK/516 μK $\approx$ 5. Once again, the total observing time is double the integration time to account for overheads, so we request an observing time of 2×4.5 hr = 9 hr.

In summary, we request 36 hours of observing time for the southern bubble of the Abell 2052 and 9 hours of observing time for the southern bubble of Perseus. As per M2 sensitivity guidelines (The Green Bank Observatory (2021)), we require observations last at least 1 hour for setup and calibration time and that observing sessions occur 3 hours after sunset and a half hour past sunrise.

[1] Note that the synthetic GBT observations (Fig. 2) are for use with the Penn Array Receiver on the GBT. To use with M2, this will change the map resolution and subsequent observing time calculations, however we proceed with using the simulated flux decrement (in μJy/arcmin^2) to estimate the desired sensitivity as the calculations were based on a central observing frequency of 90 GHz. This is the cause for the discrepancy in integration times from Pfrommer et al. (2005), which estimate integration times as 31 h and 2.1 h for Abell 2052 and Perseus, respectively.

References

Bîrzan, L., Rafferty, D., Brüggen, M., Botteon, A., Brunetti, G., Cuciti, V., ... Shimwell, T. (2020). Lofar observations of x-ray cavity systems. *Monthly Notices of the Royal Astronomical Society*, *496*(3), 2613–2635.

Blanton, E., Randall, S., Clarke, T., Sarazin, C., McNamara, B., Douglass, E., & McDonald, M. (2011). A very deep chandra observation of a2052: bubbles, shocks, and sloshing. *The Astrophysical Journal*, *737*(2), 99.

Cavagnolo, K. W. (2009). *Archive of Chandra cluster entropy profile tables: Abell 2052.* Retrieved from https://web.pa.msu.edu/astro/MC2/accept/clusters/890.html (accessed 02-12-2022)

Dicker, S. R., Battistelli, E. S., Bhandarkar, T., Devlin, M. J., Duff, S. M., Hilton, G., ... others (2021). Observations of compact sources in galaxy clusters using mustang2. *Monthly Notices of the Royal Astronomical Society*, *508*(2), 2600–2612.

Ebeling, H., Mullis, C. R., & Tully, R. B. (2002). A systematic x-ray search for clusters of galaxies behind the milky way. *The Astrophysical Journal*, *580*(2), 774.

Fabian, A., Sanders, J., Ettori, S., Taylor, G., Allen, S., Crawford, C., ... Ogle, P. (2000). Chandra imaging of the complex x-ray core of the perseus cluster. *Monthly Notices of the Royal Astronomical Society*, *318*(4), L65–L68.

Hlavacek-Larrondo, J., Li, Y., & Churazov, E. (2022). Agn feedback in groups and clusters of galaxies. *arXiv preprint arXiv:2206.00098*.

Mason, B. (2021). *MUSTANG-2.* Retrieved from https://www.gb.nrao.edu/mustang/ (accessed 02-12-2022)

McDonald, M., Gaspari, M., McNamara, B., & Tremblay, G. (2018). Revisiting the cooling flow problem in galaxies, groups, and clusters of galaxies. *The Astrophysical Journal*, *858*(1), 45.

Mroczkowski, T., Nagai, D., Basu, K., Chluba, J., Sayers, J., Adam, R., ... others (2019). Astrophysics with the spatially and spectrally resolved sunyaev-zeldovich effects. *Space Science Reviews*, *215*(1), 1–60.

Orlowski-Scherer, J., Haridas, S. K., Di Mascolo, L., Sarmiento, K. P., Romero, C. E., Dicker, S., ... others (2022). Gbt/mustang-2 9 resolution imaging of the sz effect in ms0735. 6+ 7421-confirmation of the sz cavities through direct imaging. *Astronomy & Astrophysics*, *667*, L6.

Pfrommer, C., Ensslin, T. A., & Sarazin, C. L. (2005). Unveiling the composition of radio plasma bubbles in galaxy clusters with the sunyaev-zel'dovich effect. *Astronomy & Astrophysics*, *430*(3), 799–810.

Romero, C. (2021a). *MUSTANG-2 mapping speeds.* Retrieved from https://greenbankobservatory.org/wp-content/uploads/2021/04/MUSTANG_2_Mapping_Speeds_Public.pdf (accessed 02-12-2022)

Romero, C. (2021b). *MUSTANG-2 overview, requirements.* Retrieved from https://greenbankobservatory.org/science/gbt-observers/mustang-2/mustang-2-overview-requirements/ (accessed 02-12-2022)

Seward, F. D., & Charles, P. A. (2010). *Exploring the x-ray universe.* Cambridge University Press.

The Green Bank Observatory. (2021). *MUSTANG-2.* Retrieved from https://greenbankobservatory.org/science/gbt-observers/mustang-2/ (accessed 02-12-2022)

Yang, H.-Y. K., Gaspari, M., & Marlow, C. (2019). The impact of radio agn bubble composition on the dynamics and thermal balance of the intracluster medium. *The Astrophysical Journal*, *871*(1), 6.